Article

Spin Density and Coenzyme M Coordination Geometry of the ox1 Form of Methyl-Coenzyme M Reductase: A Pulse EPR Study

Jeffrey Harmer, Cinzia Finazzo, Rafal Piskorski, Carsten Bauer, Bernhard Jaun, Evert C. Duin, Meike Goenrich, Rudolf K. Thauer, Sabine Van Doorslaer, and Arthur Schweiger

J. Am. Chem. Soc., **2005**, 127 (50), 17744-17755• DOI: 10.1021/ja053794w • Publication Date (Web): 22 November 2005

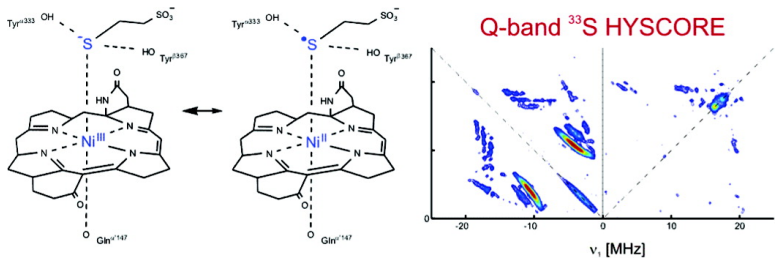

More About This Article

Additional resources and features associated with this article are available within the HTML version:

- Supporting Information
- Links to the 9 articles that cite this article, as of the time of this article download
- Access to high resolution figures
- Links to articles and content related to this article
- Copyright permission to reproduce figures and/or text from this article

View the Full Text HTML

J|A|C|S
ARTICLES
Published on Web 11/22/2005

Spin Density and Coenzyme M Coordination Geometry of the ox1 Form of Methyl-Coenzyme M Reductase: A Pulse EPR Study

Jeffrey Harmer,*,† Cinzia Finazzo,† Rafal Piskorski,‡ Carsten Bauer,‡ Bernhard Jaun,‡ Evert C. Duin,§,|| Meike Goenrich,§ Rudolf K. Thauer,§ Sabine Van Doorslaer,†,⊥ and Arthur Schweiger*,†

Contribution from the Physical Chemistry, ETH Zurich, CH-8093 Zurich, Switzerland, Organic Chemistry, ETH Zurich, CH-8093 Zurich, Switzerland, and Max-Planck-Institut für terrestrische Mikrobiologie and Laboratorium für Mikrobiologie, Fachbereich Biologie, Philipps-Universität, Karl-von-Frisch-Strasse, D-35043 Marburg, Germany

Received June 9, 2005; E-mail: harmer@esr.phys.chem.ethz.ch; schweiger@esr.phys.chem.ethz.ch

Abstract: Methyl-coenzyme M reductase (MCR) catalyses the reduction of methyl-coenzyme M (CH_3-S-CoM) with coenzyme B (H-S-CoB) to CH_4 and CoM-S-S-CoB in methanogenic archaea. Here we present a pulse EPR study of the "ready" form MCR_{ox1}, providing a detailed description of the spin density and the coordination of coenzyme M (CoM) to the Ni cofactor F_{430}. To achieve this, MCR was purified from cells grown in a ^{61}Ni enriched medium and samples were prepared in D_2O with the substrate analogue CoM either deuterated in the β-position or with ^{33}S in the thiol group. To obtain the magnetic parameters ENDOR and HYSCORE measurements were done at X- and Q-band, and CW EPR, at X- and W-band. The hyperfine couplings of the β-protons of CoM indicate that the nickel to β-proton distances in MCR_{ox1} are very similar to those in Ni(II)-$MCR_{ox1-silent}$, and thus the position of CoM relative to F_{430} is very similar in both species. Our thiolate sulfur and nickel EPR data prove a Ni−S coordination, with an unpaired spin density on the sulfur of 7 ± 3%. These results highlight the redox-active or noninnocent nature of the sulfur ligand on the oxidation state. Assuming that MCR_{ox1} is oxidized relative to the Ni(II) species, the complex is formally best described as a Ni(III) (d^7) thiolate in resonance with a thiyl radical/high-spin Ni(II) complex, $Ni^{III}-\ ^-SR \leftrightarrow Ni^{II}-\ ^{\bullet}SR$.

Introduction

Methyl-coenzyme M reductase (MCR) catalyzes the reduction of methyl-coenzyme M (CH_3-S-CoM, 2-(methylthio)ethanesulfonate) with coenzyme B (HS-CoB, 7-thioheptanoyl-threoninephosphate) to methane and CoM-S-S-CoB in the methane-forming step of the energy metabolism of methanogenic archaea.[1] The enzyme contains the nickel porphinoid cofactor F_{430}, which is the prosthetic group of MCR (Chart 1).[2−4] Different forms of the enzyme and interconversions between various MCR species are known.[5,6] Several of them, including the states MCR_{ox1}, MCR_{red1}, and MCR_{red2}, and variants of these forms are paramagnetic and EPR-visible. The oxidation state of all the red forms is Ni(I).[7−10] MCR_{red1} is the active form and has an axial Ni-based EPR spectrum characteristic of a d^9, $S = {}^1/_2$, Ni(I) complex with the unpaired electron in the $d_{x^2-y^2}$ orbital. The MCR_{red} forms accumulate in the cells when the gas mixture normally used for cell growth (80% H_2/20% CO_2) is made more reducing (100% H_2).[11,12]

The subject of this paper is the enzymatically inactive but "ready" form MCR_{ox1}, the name indicating that it can readily be reduced to active MCR_{red1}. $MCR_{ox1-silent}$ is an enzymatically inactive EPR-silent form (Ni(II), d^8, $S = 1$) that cannot readily be reduced to the active form MCR_{red1}.[13−16] However, for

† Physical Chemistry, ETH Zurich.
‡ Organic Chemistry, ETH Zurich.
§ Philipps-Universität.
|| Current address: Department of Chemistry and Biochemistry, Auburn University, AL 36849-5312, USA.
⊥ Current address: Department of Physics, SIBAC Laboratory, University of Antwerp, 2610 Wilrijk, Belgium.

(1) Thauer, R. K. *Microbiology* **1998**, *144*, 2377−2406.
(2) Pfalz, A.; Jaun, B.; Faessler, A.; Eschenmoser, A.; Jaenchen, R.; Gilles, H. H.; Diekert, G.; Thauer, R. K. *Helv. Chim. Acta* **1982**, *65*, 828−865.
(3) Jaun, B.; Pfaltz, A. *J. Chem. Soc., Chem. Commun.* **1986**, *17*, 1327−1329.
(4) Ellefson, W. L.; Whitman, W. B.; Wolfe, R. S. *Proc. Natl. Acad. Sci. U.S.A.* **1982**, *79*, 3707−3710.
(5) Mahlert, F.; Grabarse, W.; Kahnt, J.; Thauer, R. K.; Duin, E. C. *J. Biol. Inorg. Chem.* **2002**, *7*, 101−112.
(6) Mahlert, F.; Bauer, C.; Jaun, B.; Thauer, R. K.; Duin, E. C. *J. Biol. Inorg. Chem.* **2002**, *7*, 500−513.
(7) Jaun, B.; Pfaltz, A. *J. Chem. Soc., Chem. Commun.* **1986**, 1327−1329.
(8) Rospert, S.; Boecher, R.; Albracht, S. P. J.; Thauer, R. K. *FEBS Lett.* **1991**, *291*, 371−375.
(9) Goubeaud, M.; Schreiner, G.; Thauer, R. K. *Eur. J. Biochem.* **1997**, *243*, 110−114.
(10) Rospert, S.; Voges, M.; Berkessel, A.; Albracht, S. P. J.; Thauer, R. K. *Eur. J. Biochem.* **1992**, *210*, 101−107.
(11) Albracht, S. P. J.; Ankel-Fuchs, D.; Böcher, R.; Ellermann, J.; Moll, J.; Van der Zwaan, J. W.; Thauer, R. K. *Biochim. Biophys. Acta* **1988**, *955*, 86−102.
(12) Krzycki, J. A.; Prince, R. C. *Biochim. Biophys. Acta* **1990**, *1015*, 53−60.
(13) Ermler, U.; Grabase, W.; Shima, S.; Goubeaud, M.; Thauer, R. K. *Science* **1997**, *278*, 1457−1462.
(14) Shima, S.; Goubeaud, M.; Vinzenz, D.; Thauer, R. K.; Ermler, U. J. *Biochemistry* **1997**, *121*, 829−830.
(15) Grabarse, W.; Mahlert, F.; Shima, S.; Thauer R. K.; Ermler, U. *J. Mol. Biol.* **2000**, *303*, 329−344.

 10.1021/ja053794w CCC: $30.25

Chart 1. Schematic Representation of a d^7 Ni(III) Thiolate Showing F_{430}, Coenzyme M (CoM), the Two Tyrosine Fragments and $Gln^{\alpha'147}$ (from the Crystal Structure of $MCR_{ox1-silent}$)[a]

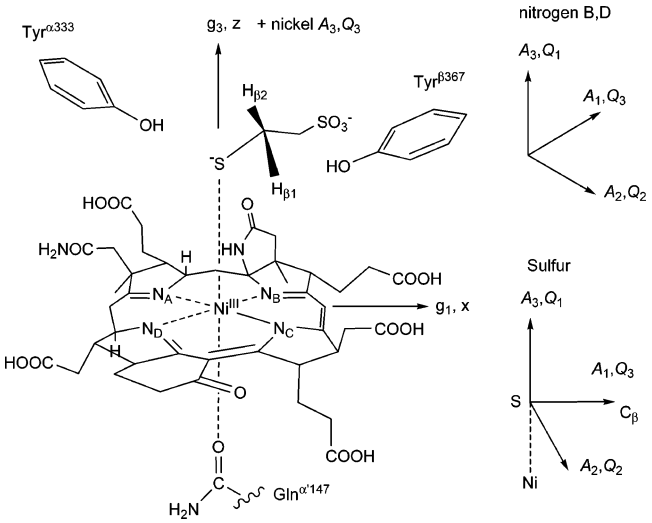

[a] CoM is orientated approximately parallel to F_{430} and is tightly bound to the protein via the SO_3^- group. The approximate orientation of the *g*, nickel, thiolate sulfur, and hydropyrrolic nitrogen hyperfine (**A**) and nuclear quadrupole (**Q**) tensors are shown.

$MCR_{ox1-silent}$ a crystal structure has been reported which shows that there are two symmetry-related active sites. Each site contains one cofactor F_{430} with the nickel being coordinated axially by the thiol(ate) sulfur of coenzyme M (CoM) and the oxygen of the glutamine residue $Gln^{\alpha'147}$ (Chart 1). The same coordination has been proposed for the "ready" form MCR_{ox1}. This is based on the observation that $MCR_{ox1-silent}$ can be directly converted into MCR_{ox1} by cryoirradiation (so-called "cryoreduction") at 77 K.[17] This proposal is consistent with X-ray absorption spectroscopy studies,[18,19] which simulated spectra from MCR_{ox1} using a model where nickel is six-coordinated with one of the axial ligands being a sulfur atom. These results, however, do not prove a covalent interaction between nickel and sulfur, information which is obtainable from EPR methods by measuring the ^{33}S hyperfine interaction.

The oxidation state of MCR_{ox1} is not known with certainty. Potential candidates are Ni(I) (d^9),[17,20] Ni(III) (d^7),[21] a Ni(III)-thiolate, or a high-spin Ni(II) ion ($S = 1$) antiferromagnetically coupled to a thiyl radical ($S = {}^1/_2$). The designation ox1 was coined because MCR_{ox1} is formed within the cells when the gas mixture used for cell growth is made less reducing (80% N_2/20% CO_2).[11,22] Moreover, addition of Ti^{III} citrate at pH 9 and 60 °C converts MCR_{ox1} to MCR_{red1}.[9] These results would suggest that MCR_{ox1} is a Ni(III) complex.

On the other hand, the oxidation state of MCR_{ox1} has also been described as Ni(I)[10,20] because MCR_{ox1} is generated from $MCR_{ox1-silent}$ by cryoirradiation[17] and because EPR and ENDOR data clearly show that MCR_{ox1} is an $S = {}^1/_2$ species with the unpaired electron predominantly in the nickel $d_{x^2-y^2}$ orbital.[10,20] The EPR spectrum of MCR_{ox1} (as well as MCR_{red1}, Ni(I)F_{430}, and Ni(I)OEiBC) is approximately axial with $g_{\|} > g_{\perp} > g_e$. This *g*-value ordering is characteristic for transition metal complexes with the unpaired electron in the $d_{x^2-y^2}$ orbital of the metal ion. Examples include d^9 Cu(II) and Ni(I) complexes in tetragonally elongated or square planar geometry.[23] Additionally, the hyperfine couplings of the four directly coordinated hydropyrrolic nitrogens of F_{430} are in the range 25−36 MHz, which is typical for complexes where the SOMO (singly occupied molecular orbital) has high $d_{x^2-y^2}$ character. In comparison, transition metal complexes with a SOMO with d_{z^2} character, such as Ni(III)$F_{430}Me_5$,[24] have a reverse *g*-value ordering, and the hyperfine couplings to the equatorial nitrogens are much smaller (~5 MHz), as for example in Cob(II)alamin.[25]

The assignment to the Ni(I) oxidation state based on a SOMO with high $d_{x^2-y^2}$ character is however not clear-cut, because both Ni(I) and Ni(III) complexes with the unpaired electron in the $d_{x^2-y^2}$ orbital are known. A $d_{x^2-y^2}$ SOMO is found in trigonal bipyramidal geometry[26] or in complexes with a strong tetragonal compression. An example of the latter is $[Ni^{III}(TPP)(CN)_2]^-$ (TPP = tetraphenylporphyrin).[27] Density functional theory (DFT) calculations on this complex and on $[Ni^{III}(F'_{430})(CH_3)(Am)]^+$ (Am = acetamide) are in agreement with a $d_{x^2-y^2}$ configuration.[21] In these complexes, the strongly σ-donating cyanide and methyl ligands apparently favor occupation of the $d_{x^2-y^2}$ orbital. Two examples of Ni(III) species with a d_{z^2} SOMO and weak axial ligands are $[Ni^{III}(TPP)(Py)_2]^+$ [27] and Ni(III)$F_{430}Me_5$.[24] In MCR_{ox1} the axial ligands are proposed to be the thiol(ate) sulfur from CoM and the oxygen from $Gln^{\alpha'147}$. Chemical intuition suggests that these ligands alone are not capable of forming a Ni(III) complex with the unpaired electron in the $d_{x^2-y^2}$ orbital. However in MCR_{ox1} the influence of the protein environment can potentially alter the ground state usually found for simpler systems and models.

Additional information concerning the oxidation state of nickel in MCR_{ox1} can be derived from X-ray Absorption Spectroscopy (XAS),[18,19] UV−vis,[24,28] and Magnetic Circular Dichroism (MCD) data.[29,30] The K-edge position of the X-ray absorption spectrum revealed that the total electron density on the nickel atom in MCR_{ox1} is similar to that in the Ni(II) forms, suggesting that part of the total electron density is spread over the ligands. Both the UV−vis and MCD spectra of MCR_{ox1} resemble those of the EPR-silent Ni(II) states. This suggests that, qualitatively, MCR_{ox1} is best described as a high-spin Ni(II)/thiyl radical complex, a Ni(III) thiolate complex, or a resonance hybrid between these two limiting cases.

(16) Grabarse, W.; Mahlert, F.; Shima, S.; Duin, E. C.; Goubeaud, M.; Sima, S.; Thauer, R. K.; Lamzin, V.; Ermler, U. *J. Mol. Biol.* **2001**, *309*, 315−330.
(17) Telser, J.; Davydov, R.; Horng, Y.-C.; Ragsdale, S. W.; Hoffman, B. M. *J. Am. Chem. Soc.* **2001**, *123*, 5853−5860.
(18) Tang, Q.; Carrington, P. E.; Horng, Y. C.; Maroney, M. J.; Ragsdale, S. W.; Bocian, D. F. *J. Am. Chem. Soc.* **2002**, *124*, 13242−13256.
(19) Duin, E. C.; Cosper N. J.; Mahlert, F.; Thauer R. K.; Scott, R. A. *J. Biol. Inorg. Chem.* **2003**, *8*, 141−148.
(20) Telser, J.; Horng, Y.-C.; Becker, D. F.; Hoffman, B. M.; Ragsdale, S. W. *J. Am. Chem. Soc.* **2000**, *122*, 182−183.
(21) Wondimagegen, T.; Ghosh, A. *J. Am. Chem. Soc.* **2001**, *123*, 1543−1544.
(22) Albracht, S. P. J.; Ankel-Fuchs, D.; Van der Zwaan, J. W.; Fontijn, R. D.; Thauer, R. K. *Biochim. Biophys. Acta* **1986**, *870*, 50−57.
(23) Pilbrow, JR. *Transition ion electron paramagnetic resonance*; Oxford: Clarendon Press: 1990.
(24) Jaun, B. *Helv. Chim. Acta* **1990**, *73*, 2209−2216.
(25) Harmer, J.; Van Doorslaer, S.; Gromov, I.; Schweiger, A. *Chem. Phys. Lett.* **2002**, *358*, 8−16.
(26) Baidya, N.; Olmstead, M. M.; Mascharak, P. K. *J. Am. Chem. Soc.* **1992**, *114*, 9666−9668.
(27) Seth, J.; Palaniappan, V.; Bocian, D. F. *Inorg. Chem.* **1995**, *34*, 2201−2206.
(28) Jaun, B. In *Metal Ions in Biological Systems, vol 29, Properties of Metal Alkyl Derivatives*; Sigel, H., Sigel, A., Eds.; Marcel Dekker: New York, 1993; pp 287−337.
(29) Duin, E. C.; Signor, L.; Piskorski, R.; Mahlert, F.; Clay, M. D.; Goenrich, M.; Thauer, R. K.; Jaun, B.; Johnson, M. K. *J. Biol. Inorg. Chem.* **2004**, *9*, 563−576.
(30) Craft, J. L.; Horng, Y.-C.; Ragsdale, S. W.; Brunold, T. C. *J. Am. Chem. Soc.* **2004**, *126*, 4068−4069.

In this contribution we determine the magnetic parameters of the hydropyrrolic nitrogens, the nickel of F_{430}, the thiol(ate) sulfur, the β-protons of CoM, and exchangeable protons. For this purpose we prepared MCR_{ox1} samples with ^{33}S and ^{2}H labeled CoM in H_2O and D_2O and purified MCR from cells of *Methanothermobacter marburgensis* grown in ^{61}Ni-enriched medium. The hyperfine and nuclear quadrupole interactions were measured with CW EPR, hyperfine sublevel correlation (HYSCORE), and pulse electron nuclear double resonance (ENDOR) experiments,[31] carried out at X- and Q-band frequencies. Combined with the *g*-values determined at W-band, these data provide an extensive collection of EPR parameters, which are used to determine the spin density and coordination environment around the nickel ion of F_{430}.

Experimental Methods

Materials and Methods. *Methanothermobacter marburgensis* is the strain deposited under DSM 2133 in the Deutsche Sammlung von Mikroorganismen und Zellkulturen (Braunschweig). Coenzyme M (2-mercaptoethanesulfonate) was obtained from Merck (Darmstadt); Coenzyme B (*N*-7-mercaptoheptanoylthreonine phosphate) was prepared from the symmetric disulfide CoB-S-S-CoB by reduction with $NaBH_4$.[32,33] Polysulfide solutions were prepared from elemental sulfur and sodium sulfide at pH 8.5.[34,35] The isotope ^{61}Ni was obtained from Campro Scientific (Berlin, Germany), with 86.6% purity. Elemental ^{61}Ni (100 mg = 1.64 mmol) was dissolved in 30 mL of 25% HCl. All other routine chemicals were obtained from Fluka, Aldrich, J. T. Baker, and Merck and were used without further purification. DMF was freshly distilled under vacuum at ca. 10 mbar and 40 °C over a fractionating column (110 cm) packed with glass beads. The reflux ratio was 10:1, and the middle fraction (30%) of the distillate was used. Amberlite IR-120 (H^+ form, 16−45 mesh) was conditioned by washing with ethanol until the eluent was colorless, storing under 20% H_2SO_4 for 1 h, and washed with water until the eluent was neutral. Flash-column chromatography was carried out on Fluka silica gel 60 (230−400 mesh ASTM). RP-HPLC was performed with an Atlantis dC_{18} 5 μm column, 19 mm × 50 mm with the following gradient program: 100% H_2O → 23 min, H_2O−acetonitrile (1:1) → 26 min, 100% acetonitrile → 36 min. The UV−vis detector was set to 220 nm.

Synthesis of Ammonium [2,2-$^2H_2$]-2-Mercaptoethanesulfonate (1) [[2,2-$^2H_2$]-Coenzyme M (NH_4^+-Form)]. A. Ammonium Ethyl Sulfoacetate (2). A solution of 2.52 g of sodium sulfite (20 mmol) in 8 mL of water was cooled with an ice bath and stirred while a solution of ethyl bromoacetate (20 mmol) in ethanol (4 mL) was added dropwise. The mixture was heated briefly to 50 °C and then evaporated to dryness. The solid residue was dissolved in 18 mL of hot acetic acid−ethyl acetate (2:1), and the hot solution was immediately filtered through Celite. The product was precipitated by dilution with ethyl acetate[36] and isolated by centrifugation. It was converted into the ammonium salt by dissolving in water, acidification with Amberlite IR-120 to pH 1, filtration, and neutralization with cold concentrated NH_3(aq). After lyophilization, the product was dissolved in a small volume of ethanol, precipitated by diethyl ether, centrifuged, and dried. The resulting solid contained 32% of **2** (according to ^1H NMR comparison with added standard) as well as inorganic salts, which did not harm the next steps and were only removed by chromatography of **6**. The yield based on ^1H NMR was 21%. ^1H NMR (D_2O, 300 MHz): δ 1.28 (*t*, 3 H,), 3.94 (*s*, 2 H), 4.24 (*q*, 2H). ^{13}C NMR (D_2O, 100 MHz): δ 15.88, 58.76, 65.52, 169.71. ESI-MS: *m*/*z* 169.9 (2), 167.9 (2), 166.8 (100). IR (KBr): 2985, 2920, 1734, 1400, 1371, 1336, 1216, 1070.

B. Ammonium [2,2-$^2H_2$]-2-Hydroxyethanesulfonate (3). Under nitrogen, sodium borodeuteride (1.05 g; 25 mmol) and 25 mL of diglyme were placed in a round-bottom two-neck flask fitted with a stirrer. After sodium borodeuteride was dissolved, 2.18 g of finely ground lithium bromide (25 mmol) were added and the mixture was stirred for 30 min. **2** (4 mmol) was added to the reaction mixture and stirred at 100 °C for 3 h under nitrogen.[37] After cooling to rt, 20 mL of methanol and 20 mL of water were added and the pH was adjusted to 11 with 1.0 M NaOH. After acidification with Amberlite IR-120 and filtration, 70 mL of methanol were added and the resulting solution was evaporated to dryness. Addition and evaporation of methanol (70 mL) was repeated 5 times.[38] Finally, the sample was dissolved in water, acidified with Amberlite IR-120, filtered, treated with cold concentrated NH_3(aq) to pH 7, and lyophilized. The crude product was dissolved in methanol, separated from insoluble solids by filtration, precipitated from diethyl ether, centrifuged, and dried to give 0.38 g (65%) of a white solid. ^1H NMR (D_2O, 300 MHz): δ 3.13 (*s*). ^{13}C NMR (D_2O, 100 MHz): δ 55.42. ESI-MS: *m*/*z* 129 (5), 128 (10), 127 (100). IR (KBr): broad 3450−3200, 2222, 2119, 1188, 1056.

C. Ammonium [2,2-$^2H_2$]-2-Bromoethanesulfonate (4). 3 (1.6 mmol) and aqueous hydrobromic acid (48%; 45 mL) were stirred at 130 °C for 3 h.[39] The reaction mixture was evaporated to dryness, the solid residue was dissolved in water, acidified with Amberlite IR-120 to pH 1, filtered, treated with cold concentrated NH_3(aq) to pH 7 and lyophilized. According to the ^1H NMR, the crude reaction product still contained 70% of **3**. Pure **4** could be isolated after chromatography on silica gel with 2-propanol−water−concentrated NH_3 (8:1:1) as an eluent. ^1H NMR (D_2O, 300 MHz): δ 3.42 (*s*). ^{13}C NMR (D_2O, 100 MHz): δ 55.71. ESI-MS: *m*/*z* 193.0 (4), 192.0 (10), 191.0 (96), 190.0 (36), 189.0 (100). IR (KBr): broad 3100−2900, 2267, 2089, 1461, 1400, 1272, 1172, 1044, 778.

D. Ammonium [2,2-$^2H_2$]-2-Thiocyanoethanesulfonate (5). 4 (1.7 mmol) was dissolved in 24 mL of dried DMF, 598 mg of potassium thiocyanate (6.08 mmol) were added, and the mixture was kept at 100 °C for 4 h. The solvent was evaporated to dryness, and the sample was dissolved in water, acidified with Amberlite IR-120 to pH 1, filtered, treated with cold concentrated NH_3(aq) to pH 7, and lyophilized. The product was dissolved in methanol and precipitated from diethyl ether, centrifuged, and dried giving 0.25 g (80%) of an off-white solid. ^1H NMR (D_2O, 300 MHz): δ 3.36 (*s*). ^{13}C NMR (D_2O, 100 MHz): δ 39.75, 117.11. ESI-MS: *m*/*z* 170.1 (9), 169.1 (16), 168.1 (100).

E. Diammonium Bis([2,2-$^2H_2$]-2-mercaptoethanesulfonate) (6). 5 (1.4 mmol) was dissolved in 20 mL of water, 2.8 g potassium carbonate (60 mmol) were added, and the solution was kept at 60 °C for 45 min. The reaction mixture was diluted with 100 mL of water, kept over 160 mL of Amberlite IR-120 for 2 h, filtered, treated with cold concentrated NH_3(aq), and lyophilized to give 0.39 g (88%) of a white solid. The product was further purified by RP-HPLC. ^1H NMR (D_2O, 300 MHz): δ 3.28 (*s*). ^{13}C NMR (D_2O, 100 MHz): δ 50.37. ESI-MS: *m*/*z* 287.8 (2), 286.7 (7), 285.9 (11), 284.8 (42), 283.7 (22), 282.7 (6), 141.8 (100). IR (KBr): 3144, 2056, 1400, 1272, 1189, 1167, 689.

F. Ammonium [2,2-$^2H_2$]-2-Mercaptoethanesulfonate (1). 50 mg of **6** (0.16 mmol) were dissolved in 3.2 mL of anaerobic water under nitrogen, 493 mg 1,4-dithio-D,L-threitol (20 equiv) were added, and the mixture was kept at 60 °C for 2 h under nitrogen. The mixture was extracted 4 times with dichloromethane, and the aqueous phase was acidified with Amberlite IR-120 to pH 1, filtered, adjusted to pH 7

(31) Schweiger, A.; Jeschke, G. *Principles of Pulse Electron Paramagnetic Resonance;* Oxford University Press: Oxford, 2001.
(32) Kobelt, A.; Pfaltz, A.; Ankel-Fuchs, D.; Thauer, R. K. *FEBS Lett.* **1987**, *214*, 265−268.
(33) Ellermann, J.; Hedderich, R.; Böcher, R.; Thauer, R. K. *Eur. J. Biochem.* **1988**, *172*, 669−677.
(34) Klimmek, O.; Kröger, A.; Steudel, R.; Holdt, G. *Arch. Microbiol.* **1991**, *155*, 177−182.
(35) Schauder, R.; Mueller, E. *Arch. Microbiol.* **1993**, *160*, 377−382.
(36) Oliver, J. E.; DeMilo, A. B. *Synthesis* **1975**, *5*, 321−322.
(37) Brown, H. C.; Mead, E. J.; Rao, B. C. S. *J. Am. Chem. Soc.* **1955**, *77*, 6209−6213.
(38) Hicks, K. B.; Simpson, G. L.; Bradbury, A. G. W. *Carbohydr. Res.* **1986**, *147*, 39−48.
(39) Rumpf, P. *Bull. Soc. Chim. Fr.* **1938**, *5*, 871−888.

with cold concentrated NH_3(aq), and lyophilized. The crude product was recrystallized from ethanol. The product was dissolved in methanol, precipitated in diethyl ether, centrifuged, and dried to give 22 mg (44%) of a white solid. It was stored under argon at −20 °C. On basis of the ^{1}H NMR the deuteration of **1** was >90%. ^{1}H NMR (D_2O, 400 MHz): δ 3.05 (overlapping *m*, 0.12 H, $-CH_2CHD-$ and $-CH_2CH_2-$), 3.27 (*s*, 2 H, $-CH_2CD_2-$), 3.29 (*s*, 0.37 H, $-CH_2CHD-$). ^{2}H NMR (H_2O, 61.42 MHz): δ 2.75 (*s*). ^{13}C NMR (D_2O, 100 MHz): δ 34.12 (*1:2:3:2:1*, $-CH_2CHD-$), 34.34 (*1:1:1*, $-CH_2CD_2-$), 53.05 (*s*, $-CH_2CD_2-$), 53.13 (*s*, $-CH_2CHD-$), 53.22 (*s*, $-CH_2CH_2-$). ESI-MS: *m*/*z* 145.0 (5), 144.0 (8), 143.0 (100), 142.0 (20).

Synthesis of Ammonium [^{33}S]-2-Mercaptoethanesulfonate (7) [2-^{33}S]-Coenzyme M (4, NH_4^+-Form)]. A. Diammonium Bis([^{33}S]-2-mercaptoethanesulfonate) (8).[40] [$^{33}S_8$]-S_8 was purchased from *Campro Scientific*, Berlin, Germany. The analysis of the isotopic purity of [$^{33}S_8$]-S_8 was established by the *Kurchatov Institute*, Moscow, Russia (isotopic purity: 99.79%; purity: >99.95%). 48.1 mg (0.182 mmol) of rhombic sulfur $^{33}S_8$ and 114 mg (1.75 mmol) of finely ground potassium cyanate were suspended in 9.0 mL of ethanol (previously degassed by three freeze−pump−thaw cycles) under nitrogen and refluxed for 4 h giving a clear solution. The solvent was evaporated, and the solid was dried under high vacuum (HV) giving 154.7 mg of the product (yield 99%). The potassium thiocyanate was suspended in 5 mL of DMF, 307 mg (1.46 mmol) of sodium 2-bromoethylsulfonate were added, and the suspension was stirred under nitrogen at 120 °C for 4 h. The solvent was evaporated giving 324 mg of solid residue which was dissolved in 10 mL of anaerobic water. Potassium carbonate (1.40 g, 5 mmol) was added, and the solution was kept at 60 °C for 45 min, diluted with 50 mL water, acidified with Amberlite IR-120 to pH 1, filtered after standing for 12 h, neutralized with cold concentrated NH_3(aq), and lyophilized. The solid was dissolved in methanol/water (19:1) and precipitated from diethyl ether. The resulting suspension was stirred for 1 h, centrifuged, and decanted, and the solid product was washed with ether and dried. **8** was further purified with RP-HPLC. ^{1}H NMR (CD_3OD, 400 MHz): δ 3.08 (*m*, 4 H), 3.14 (*m*, 4 H). ^{13}C NMR (CD_3OD, 100 MHz): δ 33.98, 52.44.

B. Ammonium [^{33}S]-2-Mercaptoethanesulfonate (7). 45 mg of **8** (0.14 mmol) were dissolved in 7.5 mL of anaerobic water in a flask under nitrogen, 1.15 g of 1,4-dithio-D,L-threitol were added, and the mixture was heated to 60 °C for 2 h under nitrogen. After cooling to rt, the mixture was extracted 7 times with dichloromethane, and the aqueous phase was acidified with Amberlite IR-120 to pH 1, filtered, treated with cold concentrated NH_3(aq) to pH 7, and lyophilized. The crude product was recrystallized from hot ethanol and dried to give 42 mg (93%) of a white solid. The total yield from $^{33}S_8$ was 88%. It was stored under argon at −20 °C. ^{1}H NMR (CD_3OD, 400 MHz): δ 2.83 (*m*, 2 H), 3.02 (*m*, 2 H). ^{13}C NMR (CD_3OD, 100 MHz): δ 20.11, 56.58. ESI-MS: *m*/*z* 142.1 (100).

MCR Purification and Samples Preparation. *M. marburgensis* cells were grown at 65 °C in a 13-L glass fermenter (New Brunswick) under 80% H_2/20% CO_2/0.1% H_2S as described.[41] In the case of *M. marburgensis* cells grown on ^{61}Ni-enriched medium, the mineral salt medium contained 20 μM $^{61}NiCl_2$ instead of 5 μM $NiCl_2$.[41] When an ΔOD_{578} of 4.5 was reached, the gas supply was switched to 100% H_2 for 30 min to induce the EPR signals MCR_{red1} and MCR_{red2} in the cells. After 30 min the cells were cooled to 10 °C within 10 min under continuous gassing and harvested anaerobically by centrifugation using a flow-through centrifuge (Hettich, centrifuge 17 RS). Approximately 70 g of wet cells were obtained. From these cells only the MCR isoenzyme I was purified.[42,43] All steps of the purification were performed in the presence of 10 mM coenzyme M and in an anaerobic chamber (Coy Instruments) filled with 95% N_2/5% H_2 as described.[41] During purification the enzyme lost its MCR_{red2} signal due to the removal of coenzyme B. In a purification generally 150 mg of active MCR in the red1c state (in 10 mL) were obtained. The purified enzyme exhibited a greenish color and showed a UV−visible spectrum at room temperature with a maximum at 385 nm (ϵ = 54 000 M^{-1} cm^{-1}) and an axial EPR signal with g_z = 2.25, g_y = 2.07, and g_x = 2.06 characteristic for MCR_{red1c}. Among different MCR preparations, 0.8−0.9 spins/mol of MCR_{red1c} per mol of Ni(I)-F_{430} was obtained.

To remove coenzyme M or exchange the 10 mM Tris/HCl buffer against buffer prepared with D_2O, the purified MCR was washed and concentrated using Amicon Ultra Centrifugal Filter Devices (Millipore) with a 100-kDa molecular mass cutoff. To induce the MCR_{ox1} state, the coenzyme-free and concentrated MCR was supplemented with 30 mM of either coenzyme M, or coenzyme M in D_2O, or [2-^{33}S]-coenzyme M, or [2,2-$^2H_2$]-coenzyme M, and 30 mM coenzyme B and 5 mM freshly prepared polysulfide.

The protein concentration was determined by measuring the absorbance difference of oxidized enzyme (MCR-silent) at 420 nm using an ϵ = 44 000 M^{-1} cm^{-1} for a molecular mass of 280 000 Da.

EPR Spectroscopy (Sample Control). As a control of the sample quality and concentration, 1 to 10 diluted samples (0.35 mL) were analyzed for EPR spectra at 77 K in 0.3 cm (inner diameter) quartz tubes with 95% N_2/5% H_2 as gas phase and closed with a closed-off rubber tube. The samples contained approximately 9.6 mg of MCR (35 nmol) in 10 mM Tris/HCl pH 7.6. CW EPR spectra at X-band were recorded with a Bruker EMX-6/1 EPR spectrometer composed of an EMX 1/3 console, an ER 041 × X6 bridge with built-in ER-0410-116 microwave (mw) frequency counter, an ER-070 magnet, and an ER-4102st standard universal rectangular cavity. All spectra were recorded with an mw frequency of 9.44 GHz, an mw power incident to the cavity of 2 mW, a temperature of 77 K, a modulation frequency of 100 kHz, and a modulation amplitude of 0.6 mT. Spin quantifications were carried out under nonsaturating conditions using 10 mM copper perchlorate as a standard (10 mM $CuSO_4$; 2 M $NaClO_4$; 10 mM HCl). All signal intensities are expressed as spins per mol of F_{430}. These EPR data were used exclusively for sample quality control, and all experimental spectra shown in this paper are described below.

EPR Spectroscopy. The W-band (94.1659 GHz) CW EPR spectrum was measured at 90 K on a Bruker E680 spectrometer with an mw power of 0.1 mW, a modulation amplitude of 0.5 mT, and a modulation frequency of 100 kHz. The field was calibrated using the two central lines from a CaO sample containing manganese ions. The X-band (9.4 GHz) CW EPR spectra were measured at 110 K on a Bruker E500 spectrometer using an mw power of 1 mW, a modulation amplitude of 0.1−0.3 mT, and a modulation frequency of 100 kHz. The field was calibrated with a Bruker 035M NMR gaussmeter.

The pulse EPR experiments were carried out at Q-band (35.3 GHz) on a home-built instrument[44] and at X-band (9.7 GHz) on a Bruker E680 spectrometer. Both instruments were equipped with a Helium gas-flow cryostat from Oxford Inc. The field-swept frozen-solution EPR spectra were recorded by integrating over the echoes created with the mw pulse sequence $\pi/2$-τ-π-τ-*echo*, with mw pulse lengths $t_{\pi/2}$ = 50 ns, t_π = 100 ns, and an interpulse delay of τ = 700 ns. The first derivative of this spectrum was calculated numerically. The ^{14}N and ^{61}Ni Davies-ENDOR spectra were measured at Q-band with the mw pulse sequence π-*T*-$\pi/2$-τ-π-τ-*echo*, with mw pulses of length $t_{\pi/2}$ = 30 ns and t_π = 60 ns, and τ = 220 ns. A radio frequency pulse of length 32 μs and variable frequency ν_{ENDOR} was applied during time

(40) The outline of this synthesis has been reported in our earlier communication (Finazzo, C.; Harmer, J.; Bauer, C.; Jaun, B.; Duin, E. C.; Mahlert, F.; Goenrich, M.; Thauer, R. T.; Van Doorslaer, S.; Schweiger, A. *J. Am. Chem. Soc.* **2003**, *125*, 4988−4989).

(41) Mahlert, F.; Grabarse, W.; Kahnt, J.; Thauer, R. K.; Duin, E. C. *J. Biol. Inorg. Chem.* **2002**, *7*, 101−112.

(42) Rospert, S.; Linder, D.; Ellermann, J.; Thauer, R. K. *Eur. J. Biochem.* **1990**, *194*, 871−877.

(43) Bonacker, L. G.; Baudner, S.; Mörschel, E.; Böcher, R.; Thauer, R. K. *Eur. J. Biochem.* **1993**, *217*, 587−595.

(44) Gromov, I.; Shane, J.; Forrer, J.; Rakhmatoullin, R., Rozentzwaig, Y.; Schweiger, A. *J. Magn. Reson.* **2001**, *149*, 196−203.

T. The ^{1}H Davies-ENDOR spectra were measured at Q-band with mw pulses of length $t_{\pi/2} = 40$ ns and $t_\pi = 80$ ns, $\tau = 196$ ns, and a radio frequency pulse of length 15 μs.

HYSCORE experiments employed the pulse sequence $\pi/2$-τ-$\pi/2$-t_1-π-t_2-$\pi/2$-τ-*echo*. At Q-band the following parameters were used: mw pulses of lengths $t_{\pi/2} = t_\pi = 16$ ns, starting times 96 ns for t_1 and t_2, and time increments $\Delta t = 12$ ns (data matrix 200 × 200). Spectra with different τ values were recorded. At X-band the parameters were: mw pulses of lengths $t_{\pi/2} = t_\pi = 16$ ns, starting times 96 ns for t_1 and t_2, $\Delta t = 20$ ns (data matrix 450 × 450). An eight-step phase cycle was used to remove unwanted echoes. The HYSCORE data were processed with MATLAB 7.0 (The MathWorks, Inc.). The time traces were baseline corrected with an exponential, apodized with a Gaussian window, and zero filled. After a two-dimensional Fourier transformation absolute-value spectra were calculated. Spectra recorded with different τ values were added to eliminate τ-dependent blind spots.

EPR Simulations. The EPR and Davies-ENDOR spectra were simulated with the program EasySpin.[45] HYSCORE spectra were simulated with a program written in-house,[46] or if only the cross-peak frequencies (and not the intensities) were of interest, by exact diagonalization of the spin Hamiltonian. Simulated spectra were generally fitted to experimental spectra using the Newton−Gauss−Levenberg/Marquardt (NGL/M) algorithm. To help find the global minimum, the NGL/M algorithm was used in conjunction with a large set of initial guesses, and the best fit was then found. In the case of the four nitrogens, data along g_3 were fitted while keeping those along g_1 and g_2 fixed, and vice versa, to reduce the number of parameters that were optimized at each cycle.

EPR Theory. The spin Hamiltonian for an $S = {}^1/_2$ system coupled to i nuclei, in frequency units, is given by

$$\mathrm{H} = (\beta_e/h)\mathbf{S}\mathbf{g}\mathbf{B}_0 + \Sigma\,\mathbf{S}\mathbf{A}_i\mathbf{I}_i - (\beta_n/h)\Sigma\, g_{i,n}\mathbf{I}_i\mathbf{B}_\mathbf{0} + \Sigma\,\mathbf{I}_i\mathbf{Q}_i\mathbf{I}_i \quad (1)$$

where the terms describe the electron Zeeman interaction, the hyperfine interactions, the nuclear Zeeman interactions, and the nuclear quadrupole interactions (for nuclei with $I > {}^1/_2$).

The ENDOR spectrum of a nucleus with spin $I = {}^1/_2$ at a single orientation consists of two transitions. For $\mathbf{B}_0$ along one of the hyperfine principal axes the frequencies are given by $\nu = |\nu_I \pm ({}^1/_2)A_i|$, where ν_I is the nuclear Zeeman frequency and A_i is one of the principal hyperfine values. For a nucleus with spin $I = {}^3/_2$ (^{33}S or ^{61}Ni) the ENDOR spectrum at a single orientation consists of six single-quantum transitions. For the magnetic field along one of the principal axes these frequencies are given by $\nu = |\nu_I \pm ({}^1/_2)A_i + ({}^3/_2)Q_i(2m_I + 1)|$, where Q_i denotes a principal value of the **Q** tensor along the principal axis and m_I is the nuclear spin quantum number ($m_I = -{}^3/_2, -{}^1/_2, {}^1/_2$). In HYSCORE, all six nuclear transitions in each electron spin manifold need to be considered; three single-quantum (sq) transitions with $|\Delta m_I| = 1$, two double-quantum (dq) transitions with $|\Delta m_I| = 2$, and one triple-quantum transition with $|\Delta m_I| = 3$.[47] A HYSCORE spectrum contains cross-peaks between the nuclear frequencies in one electron spin manifold with the nuclear frequencies in the other electron spin manifold. Generally, only a few of the possible 36 (6 × 6) cross-peaks are observed.

Results

CW EPR Spectra: Figure 1A shows the W-band EPR spectrum of [^{33}S-CoM]-MCR$_{ox1}$, along with a simulation using $g_1 = 2.1527(2)$, $g_2 = 2.1678(2)$, and $g_3 = 2.2312(2)$, and an isotropic Gaussian line width of 190 MHz. These *g*-values are in good agreement with those found at X-band but are more accurate due to the higher resolution at W-band. There is an impurity in the spectrum which is marked by three *; it contributes ~15% of the signal intensity with *g*-values of 2.190, 2.202, 2.218. Note that the impurity is only present in the [^{33}S-CoM]-MCR$_{ox1}$ samples. While at W-band the hyperfine structure is lost due to *g*-strain, at X-band the spectra show a well-resolved hyperfine structure. Figure 1B shows the second derivative X-band CW EPR spectrum of MCR$_{ox1}$ (top), [^{33}S-CoM]-MCR$_{ox1}$ (middle), and ^{61}Ni-MCR$_{ox1}$ (bottom). The first harmonic spectra are given in Figure S1. All features of the MCR$_{ox1}$ spectrum could be accounted for using the *g*-values obtained from W-band and four nitrogen hyperfine interactions (see Table 1).

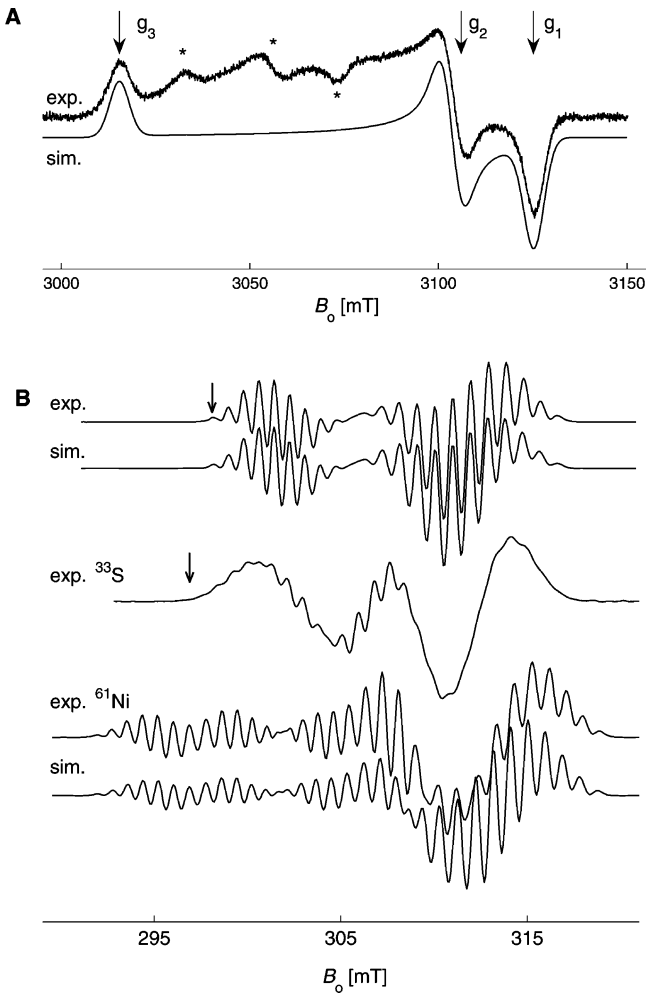

Figure 1. CW EPR spectra of frozen solutions of MCR$_{ox1}$, experimental (exp.) and simulated (sim.). (A) W-band spectrum of [^{33}S-CoM]-MCR$_{ox1}$ measured at 90 K. An impurity in the middle of the spectrum is marked with three *. (B) X-band spectra (second derivative) of MCR$_{ox1}$ measured at 110 K (top), [^{33}S-CoM]-MCR$_{ox1}$ (middle), and ^{61}Ni-MCR$_{ox1}$ (bottom). The arrows in B (top and middle) identify the lower edge of each spectrum which highlights the ^{33}S hyperfine splitting.

The spectrum of [^{33}S-CoM]-MCR$_{ox1}$ (middle) shows additional broadening due to the ^{33}S hyperfine interaction (nuclear spin $I = {}^3/_2$). However, because of the aforementioned impurity (see Figure 1A) reliable information can only be obtained from the high- and low-field edges of the spectrum. At the low-field edge of the [^{33}S-CoM]-MCR$_{ox1}$ spectrum simulation gives a range of possible values for the ^{33}S hyperfine coupling along g_3 of $8 < A_3(^{33}\mathrm{S}) < 28$ MHz, while at the high-field end only an upper limit from line-broadening effects can be deduced, $A_{1,2}(^{33}\mathrm{S}) < 25$ MHz.

(45) See http://www.esr.ethz.ch.
(46) Madi, Z.; Van Doorslaer, S.; Schweiger, A. *J. Magn. Reson.* **2002**, *154*, 181−191.
(47) Gutjahr, M.; Böttcher, R.; Pöppl, A. *Appl. Magn. Reson.* **2002**, *22*, 401−414.

Table 1. Hyperfine and Nuclear Quadrupole Parameters of MCR_{ox1}

nucleus	description	$\|A_1\|$ [MHz]	$\|A_2\|$ [MHz]	$\|A_3\|$ [MHz]	$[\alpha,\beta,\gamma]^b$ degrees	$\|e^2qQ/h\|^c$ [MHz]	η^c	$[\alpha,\beta,\gamma]^b$ degrees
$^{14}N_1$	hydropyrrolic	26.7 ± 1	23.4 ± 1	25.0 ± 0.5	45,0,0	3.5 ± 0.5	0.16 ± 0.05	45,90,0
$^{14}N_2$	hydropyrrolic	30.1 ± 1	24.9 ± 1	24.0 ± 0.5	135,0,0	3.4 ± 0.5	0.12 ± 0.05	135,90,0
$^{14}N_3$	hydropyrrolic	31.5 ± 1	26.7 ± 1	24.5 ± 0.5	225,0,0	2.9 ± 0.5	0.16 ± 0.05	225,90,0
$^{14}N_4$	hydropyrrolic	35.6 ± 1	26.4 ± 1	26.5 ± 0.5	315,0,0	2.9 ± 0.5	0.21 ± 0.05	315,90,0
^{61}Ni	F_{430}	39 ± 2	42 ± 2	132 ± 1	0,0,0	22 ± 2	0.02 ± 0.05	0,0,0
^{33}S	thiol-CoM	10 ± 3	24 ± 3	17 ± 3	0,−5,5	36 ± 2	0.1 ± 0.1	0,75,15
$^1H^a$	β1-CoM[d]	-5.5 ± 0.4	-6.6 ± 0.4	6.1 ± 0.4	−93,125,14	0.18 ± 0.05	0.1 ± 0.1	0,12,34
$^1H^a$	β2-CoM[d]	-3.5 ± 0.4	-3.2 ± 0.4	2.2 ± 0.4	−91,36,−155	0.18 ± 0.05	0.1 ± 0.1	180,119,82
$^1H^a$	ex1-D_2O	5.0 ± 0.5	8.0 ± 0.5	9.9 ± 0.5	87,80,105	0.2 ± 0.1		
$^1H^a$	ex2-D_2O		<4			~0.3		

[a] Proton hyperfine couplings are given (^1H, $I = {}^1/_2$), to get the corresponding deuterium hyperfine couplings divide by 6.5. Nuclear quadrupole parameters are for deuterium (^2H, $I = 1$). [b] Euler angles define the passive rotation of the hyperfine or nuclear quadrupole principal axis system into the *g*-matrix principal axis system, $\boldsymbol{A} = \mathbf{R}(\alpha,\beta,\gamma)\boldsymbol{A}_{\text{diagonal}}\mathbf{R}^+(\alpha,\beta,\gamma)$. [c] Nuclear quadrupole interactions $\kappa = (e^2qQ/h)/(4I(2I-1))$ and asymmetry parameters $\eta = (Q_x - Q_y)/Q_z$ with $Q_x = -\kappa(1-\eta)$, $Q_y = -\kappa(1+\eta)$, and $Q_z = 2\kappa$. [d] The sign of the hyperfine coupling is based on expectations from the point-dipole model.

In Figure 1B (bottom) the ^{61}Ni-MCR_{ox1} spectrum shows clear splittings caused by the nickel hyperfine interaction, with the largest coupling along the $\mathbf{g}_3$ axis ($d_{x^2-y^2}$ SOMO with $\mathbf{g}_3$ perpendicular to F_{430}, Chart 1). A simulation of this spectrum, in combination with ENDOR data (see below), allowed the ^{61}Ni hyperfine tensor to be determined (Table 1). Note that the simulation is the sum of 86.6% ^{61}Ni ($I = {}^3/_2$) and 13.4% ^{59}Ni ($I = 0$) spectra.

^{61}Ni and ^{14}N ENDOR: X- and Q-band Davies-ENDOR spectra increased the accuracy of the ^{61}Ni hyperfine data. Moreover the spectra enabled the nuclear quadrupole interaction to be estimated. Figure 2 shows the Q-band spectra and their simulations using parameters for the nickel and hydropyrrolic nitrogens listed in Table 1 (the X-band spectra are shown in Figure S2). For observer positions close to the low-field end of the EPR spectrum only nitrogen signals are observed in the rf range investigated (Figure 2D−F); here the nickel hyperfine interaction could be determined accurately from the CW EPR spectrum (Figure 1B, bottom). At observer positions near the high-field end, signals of both nitrogen and nickel contribute to the ENDOR spectra (Figure 2A−C). The ^{61}Ni peaks in the "single-crystal"-like spectrum, Figure 2A, are approximately centered at half the hyperfine coupling, ~40 MHz/2, split by twice the nuclear Zeeman frequency (3.8 MHz × 2), and split by the nuclear quadrupole coupling. Using the values in Table 1 the six single-quantum transitions along the $\mathbf{g}_1$ axis are 20, 17, and 10 MHz in one electron spin manifold and 29, 25, and 19 MHz in the other electron spin manifold. The three highest frequencies can readily be seen in Figure 2A, the other three overlap with signals from the nitrogens. The peaks in Figure 2A are broadened, since at this "single-crystal" position a significant number of orientations in the $\mathbf{g}_1-\mathbf{g}_2$ plane contribute to the spectrum.

The nickel hyperfine tensor is axial within experimental error and oriented with the $\mathbf{A}_3$ axis along the $\mathbf{g}_3$ axis and the $\mathbf{A}_1$ and $\mathbf{A}_2$ axes lying in the plane of F_{430} (Chart 1). The ENDOR data allowed only two principal values Q_x and Q_y of the nuclear quadrupole interaction to be determined, the Q_z value was calculated, $Q_z = -(Q_x + Q_y)$. The nuclear quadrupole interaction is approximately axial with the axis of the largest value Q_z being collinear to $\mathbf{A}_3$.

The **g** matrix is orientated such that the $\mathbf{g}_3$ axis is perpendicular to the plane of F_{430} and the $\mathbf{g}_1$ and $\mathbf{g}_2$ axes are in the plane and approximately bisect the hydropyrrolic N−Ni−N bond angles (see Chart 1). The same **g** matrix orientation was found in Cu(II) tetraphenylporphyrin from a single-crystal study

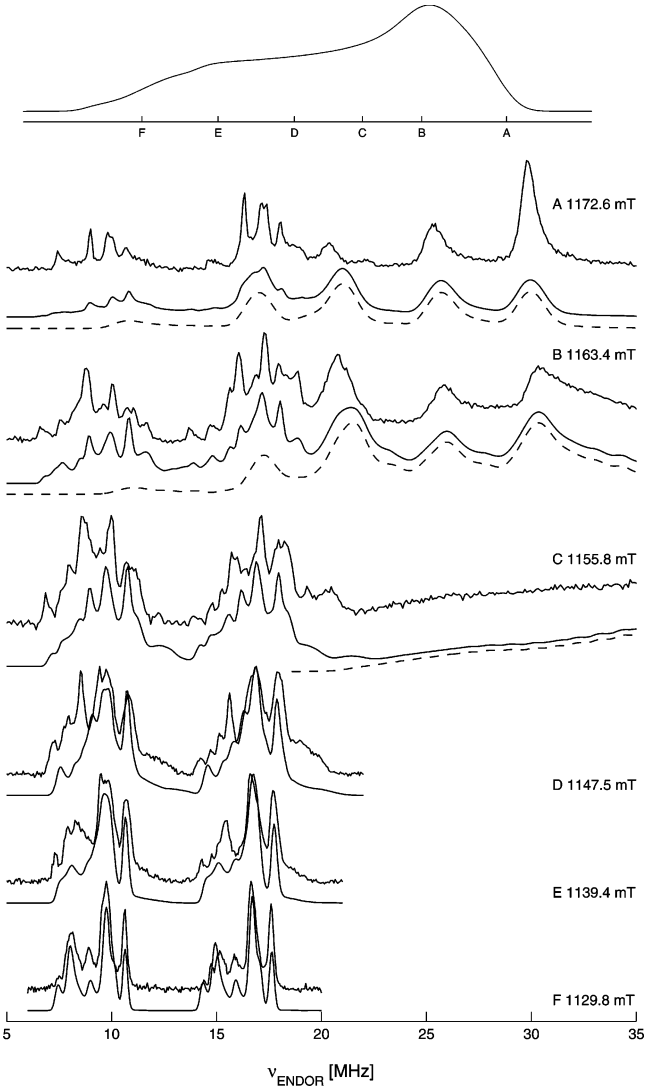

Figure 2. Q-band (35.30 GHz) Davies-ENDOR spectra of ^{61}Ni-MCR_{ox1} measured at 15 K at six field positions. At each position the upper solid line is the experimental data, and the lower solid line is the simulation, which is the sum of spectra from four ^{14}N nuclei and a ^{61}Ni nucleus. The ^{61}Ni simulation (dashed line) contributes only to spectra A−C; at the lower field positions (D−F) the peaks shift to frequencies higher than 35 MHz. Top: echo-detected EPR spectrum showing the observer positions.

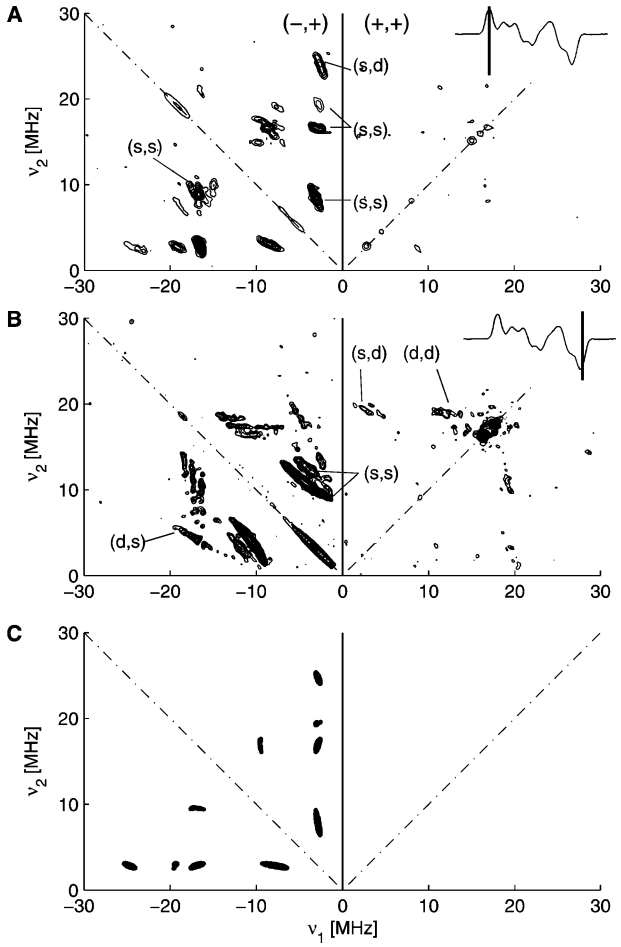

Figure 3. Q-band (35.26 GHz) HYSCORE spectra of [^{33}S-CoM]-MCR$_{ox1}$ measured at 25 K at observer position (A) 1128.9 mT, (B) 1171.9 mT. Both spectra are the sum of two τ values, 108 ns and 132 ns. Selected ^{33}S double-quantum (d) and single-quantum (s) frequencies are labeled. Insets: Echo-detected EPR spectrum (first derivative) showing the observer position of the HYSCORE spectra. (C) Simulation of A.

(again a SOMO with high $d_{x^2-y^2}$ character).[48] The simulation of hydropyrrolic nitrogen ENDOR spectra of MCR$_{ox1}$ enables the conclusion that $\mathbf{g}_1$ and $\mathbf{g}_2$ bisect the N−Ni−N bound angles;[20] it is not possible however to determine which N−Ni−N bond angle $\mathbf{g}_1$ or $\mathbf{g}_2$ bisect. From our proton CoM data we were able to tentatively make this assignment (see below).

The nitrogen ENDOR spectra were simulated with four distinct nitrogen nuclei. Given the large number of adjustable parameters (for each nitrogen five coupling parameters and six Euler angles), the error in the parameters is comparable to the relatively small difference between the nitrogen couplings, in particular in the $\mathbf{g}_1-\mathbf{g}_2$ plane. To achieve a satisfactory simulation at all observer positions, a model employing four nitrogens is needed, which shows that all four nitrogens have different couplings.

^{33}S-CoM HYSCORE: Q-band HYSCORE enabled the ^{33}S hyperfine and nuclear quadrupole tensors to be determined. Figure 3 shows a "single-crystal"-like HYSCORE spectrum recorded at the low-field edge of the EPR spectrum (A) and a HYSCORE spectrum recorded at the high-field edge of the EPR spectrum where many orientations in and around the $\mathbf{g}_1-\mathbf{g}_2$ plane contribute (B). As shown in the insets of Figure 3, both spectra are measured at positions where there is no signal from the impurity present in the [^{33}S-CoM]-MCR$_{ox1}$ sample. In Figure 3 we have labeled a selection of cross-peaks representing either single-quantum (s, $\Delta m_I = 1$) or double-quantum (d, $\Delta m_I = 2$) transitions. The assignment of these peaks is based on simulations using the ^{33}S parameters in Table 1. The simulation of the spectrum in Figure 3A is shown in Figure 3C, which plots the assigned sulfur cross-peaks when all nuclear transition intensities have unit amplitude. Figure S3 shows the simulation of Figure 3B. In the experimental spectra we confirmed that the cross-peaks are due to interactions with ^{33}S since these peaks (1) are absent in spectra of [^{32}S-CoM]-MCR$_{ox1}$, (2) are at the wrong frequencies to belong to the hydropyrrolic nitrogens (the expected cross-peak frequencies were calculated using the values in Table 1). The lack of observable signals assignable to hydropyrrolic nitrogens is expected as they have larger and less anisotropic hyperfine couplings and smaller nuclear quadrupole interactions in comparison to the ^{33}S interactions. On similar compounds (e.g., MCR$_{red2}$[49]) we could only observe signals from strongly coupled nitrogens using HYSCORE with matched pulses.[31]

In the spectrum recorded at the low-field position of the EPR spectrum (Figure 3A), single-quantum cross-peaks in the (−,+) quadrant dominate the spectrum. The HYSCORE spectrum recorded at the high-field end of the EPR spectrum (Figure 3B) has intense (s,s) cross-peaks that form two long ridges in the (−,+) quadrant. The doubling of the ridges is caused by the nuclear quadrupole splitting, whereas the length is determined by the anisotropy of the ^{33}S hyperfine interaction. Positions and lengths of these two pairs of ridges thus provide initial values for the hyperfine couplings in the $\mathbf{g}_1-\mathbf{g}_2$ plane, $A = 10-20$ MHz. In both spectra the most intense peaks occur in the (−,+) quadrant, indicating that at Q-band the sulfur hyperfine interaction is in the strong coupling regime, $|A| > 2|\nu_I| \cong 7.5$ MHz.

The ^{33}S hyperfine interaction has one small (along $\mathbf{g}_1$) and two large (along $\mathbf{g}_2$ and $\mathbf{g}_3$) principal values. These principal values are consistent with the lower and upper limits determined from the X-band CW EPR spectrum (Figure 1B, middle). The nuclear quadrupole interaction is approximately axial with the axis of the largest principal value pointing approximately along the $\mathbf{g}_1$ axis (near to the S−C_β direction, Chart 1). The large nuclear quadrupole coupling constant of $|e^2qQ/h| = 36$ MHz is within the range found in a study of a set of small diamagnetic molecules.[50]

Deuterium HYSCORE and Proton ENDOR: X-band HYSCORE was used to measure signals due to deuterium from [^{2}H$_2$-CoM]-MCR$_{ox1}$ and MCR$_{ox1}$ in D_2O. For these species X-band HYSCORE is very sensitive to deuterium as the nuclear modulation effect is large. Figure 4 shows one of the [^{2}H$_2$-CoM]-MCR$_{ox1}$ spectra and its simulation (the other six spectra and their simulations are shown in Figure S4). The most intense peaks are close to the antidiagonal at the ^{2}H Larmor frequency ($\nu^2_H = 2.07$ MHz) and are single-quantum cross-peaks. Examination of this region reveals that two nuclei, $\beta 1$ and $\beta 2$, contribute to the pattern. Nucleus $\beta 1$ manifests itself as two long ridges from 1 to 3 MHz running parallel to the antidiagonal

(48) Brown, T. G.; Hoffman, B. M. *Mol. Phys.* **1980**, *39*, 1073−1109.
(49) Finazzo, C.; Harmer, J.; Jaun, B.; Duin, E.; Mahlert, F.; Thauer, R. K.; Van Doorslaer, S.; Schweiger, A. *J. Biol. Inorg. Chem.* **2003**, *8*, 586−593.
(50) Bailey, W. C.; Gonzalez, F. M.; Castiglione, J. *Chem. Phys.* **2000**, *260*, 327−335.

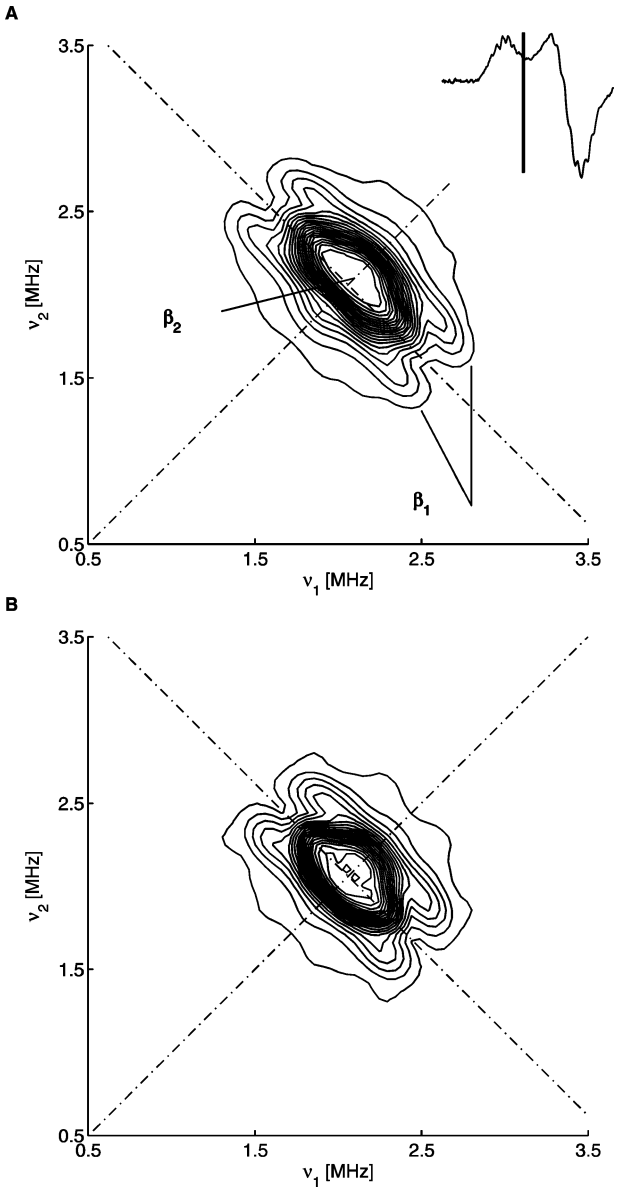

Figure 4. X-band (9.749 GHz) HYSCORE spectra of [$^2H_2$-CoM]-MCR_{ox1}. (A) Experimental spectrum measured at 20 K at observer position 317.5 mT. The pattern is assigned to single-quantum cross-peaks from the two deuterium nuclei β1 and β2 of $^2H_2$-CoM. Inset: Echo-detected EPR spectrum (first derivative) showing the observer position. (B) Simulation.

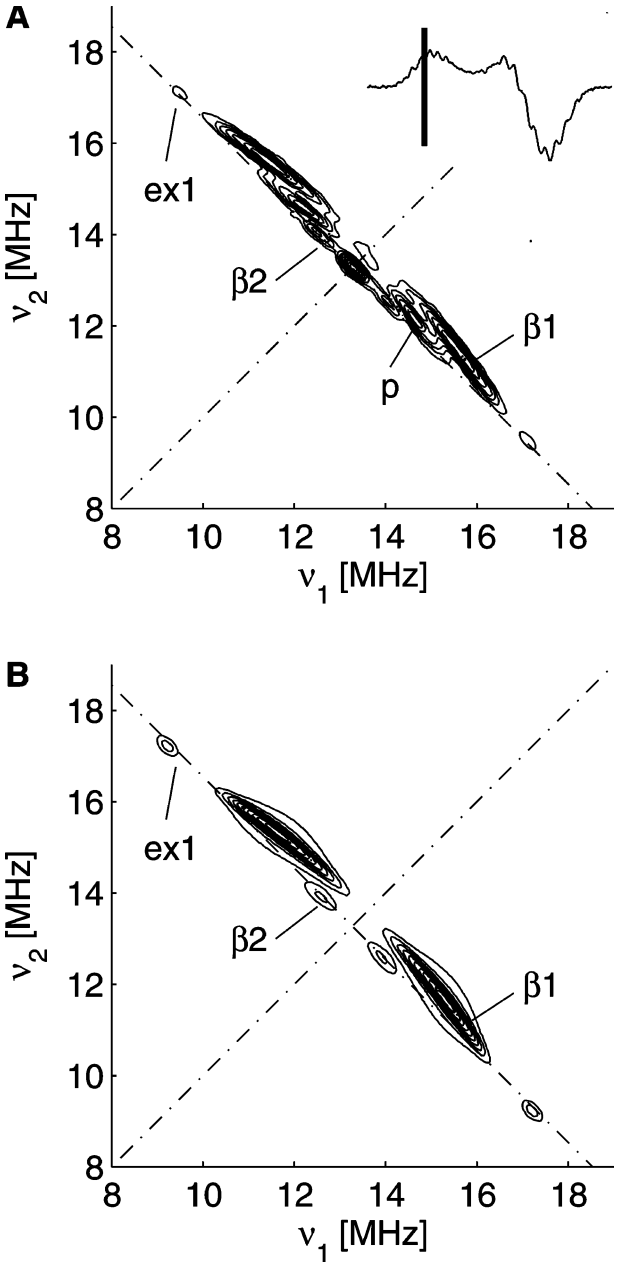

Figure 5. X-band (9.749 GHz) HYSCORE spectra of MCR_{ox1} recorded with a τ of 132 ns at 310.0 mT (g_3 observer position, see inset) (A) Experimental spectrum measured at 20 K. Signals from proton β1, β2, ex1, and p are labeled. (B) Simulation.

and split by the nuclear quadrupole interaction. Nucleus β2 has a significantly smaller hyperfine coupling and unresolved nuclear quadrupole splittings. This produces an intense peak extending along the antidiagonal from 1.7 to 2.3 MHz.

The data for the proton hyperfine interactions were refined further using ^1H HYSCORE spectra from MCR_{ox1}. In HYSCORE, the large anisotropy of the hyperfine interaction of proton β1 results in a ridge that is displaced above the antidiagonal at the ^1H Larmor frequency, with a maximum shift from the antidiagonal given by $\Delta\nu_{max} = (9T^2/32\nu_{^1H})$, where T is the dipolar contribution of an axial hyperfine tensor with principal values $-T$, $-T$, $2T$. Proton β1 is thus well resolved from the many other contributing proton signals. Figure 5 shows a ^1H HYSCORE spectrum and the corresponding simulations. Proton β1 is well-resolved and accurately described with the parameters in Table 1, proton β2 has a much smaller hyperfine anisotropy, and its signals are very close to the antidiagonal and overlap with signals from nearby protons of F_{430} and the protein. The pair of cross-peaks labeled with ex1 are assigned to an exchangeable proton(s) as described below, and the ridge labeled with a "p" has a hyperfine coupling of up to ~4 MHz and probably belongs to one of the nearest protons of F_{430} or the protein (e.g., $Gln^{\alpha'147}$).

The ^1H and ^2H HYSCORE spectra enabled us to determine the hyperfine and nuclear quadrupole parameters for the two nuclei (Table 1). To ensure that the parameters have physical significance, a model of F_{430} and CoM was used (starting from the crystal structure of $MCR_{ox1-silent}$, Chart 1). The orientations and anisotropies of the β1 and β2 proton hyperfine matrices were then calculated using the point-dipole model with spin density on the four hydropyrrolic nitrogens, the nickel, and the

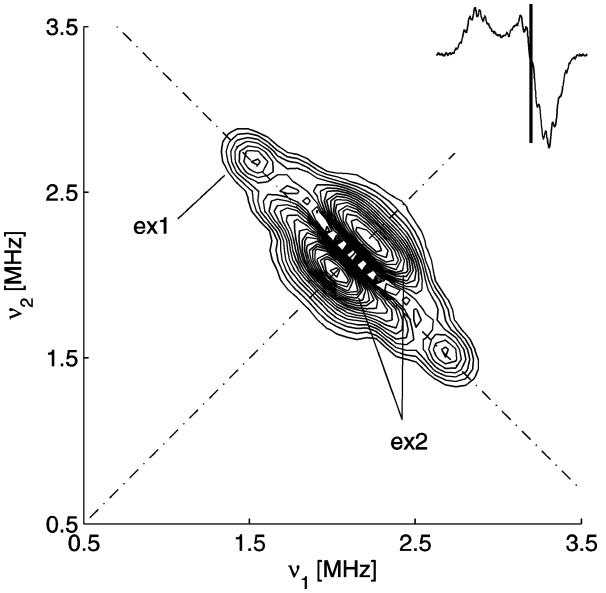

Figure 6. X-band (9.759 GHz) HYSCORE spectrum of MCR_{ox1} in D_2O measured at 20 K at observer position 321.2 mT. The cross-peaks are assigned to single-quantum transitions from exchangeable deuterium nuclei, ex1 and ex2. Inset: Echo-detected EPR spectrum (first derivative) showing the observer position.

sulfur. The spin density on these nuclei was estimated from the EPR data (see Discussion). An isotropic contribution was added to the dipolar part of the hyperfine tensor to best fit the data. The signs of the hyperfine principal values thus result from the sum of the isotropic and dipolar parts (with contributions of the general form [−1,−1,2]). The orientation of the largest deuterium nuclear quadrupole coupling was assumed to point along the carbon−deuterium bond. These initial parameters were then optimized by fitting the simulated to the experimental spectra. The simulations show that protons β1 and β2 are close to the $\mathbf{g}_1$ axis. By assuming that CoM binds to the protein via the SO_3^- group with a similar orientation to F_{430} as in $MCR_{ox1-silent}$, we were able to tentatively assign the $\mathbf{g}_1$ axis to bisect the N_B-Ni-N_C bond angle and the $\mathbf{g}_2$ axis to bisect the N_A-Ni-N_B bond angle (Chart 1). This assumption is justified because MCR_{ox1} is formed from $MCR_{ox1-silent}$ by cryoirradiation (at 77 K).

Figure 6 shows a HYSCORE spectrum from MCR_{ox1} in D_2O recorded near $\mathbf{g}_2$. This spectrum is caused by a number of deuterium nuclei that have replaced exchangeable protons. The nucleus ex1 with the strongest coupling is represented by single-quantum cross-peaks at approximately (1.5, 2.7) MHz and (2.7, 1.5) MHz, and an unresolved nuclear quadrupole splitting. Both ^2H HYSCORE and ^1H ENDOR (see below) spectra measured at different field positions allowed the EPR parameters of ex1 to be determined (Table 1). Comparison of ^1H ENDOR spectra from MCR_{ox1} in D_2O and in H_2O confirmed the hyperfine couplings and showed that ∼60% of ex1 protons were exchanged (Figure S5). The HYSCORE spectrum in Figure 6 also has two intense ridges which run parallel to the antidiagonal from (1.8, 2.4) MHz to (2.4, 1.8) MHz, and are split by ∼0.25 MHz due to the nuclear quadrupole interaction. An approximate simulation of this pattern could be obtained using a single nucleus, ex2 (Table 1). However, we stress that the pattern could well be caused by several nuclei with similar couplings. Likely candidates for exchangeable protons include the two OH tyrosine

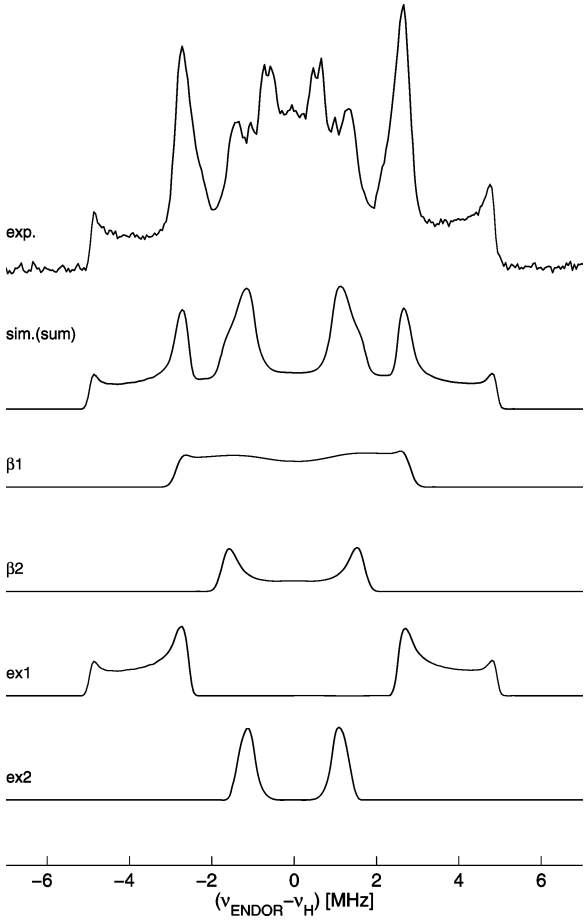

Figure 7. ^1H Q-band (35.30 GHz) Davies-ENDOR spectrum of MCR_{ox1} measured at 15 K at the observer position 1167.0 mT (near the echo maximum, see Figure 2). Experimental spectrum (exp.) and simulation (sim.), which is the sum of the four spectra of β1, β2, ex1, and ex2.

protons, exchangeable NH protons of F_{430}, and potentially protons from a water molecule near to the active site (the X-ray structure of $MCR_{ox1-silent}$ has a water molecule near CoM).

As a check of the accuracy of the hyperfine couplings obtained from the HYSCORE experiments, Q-band ^1H Davies-ENDOR spectra of MCR_{ox1} were recorded at five field positions (Figure S6). Figure 7 shows a spectrum recorded near g_2, together with simulations for the protons β1 and β2 of CoM and the exchangeable protons ex1 and ex2. Inspection of this figure convincingly supports the proton hyperfine parameters given in Table 1. It should be noted that the region of the spectra from approximately −2 MHz to +2 MHz represents the many protons from F_{430} and the surrounding protein and is thus not fully described by the simulations.

Discussion

Table 1 provides an extensive list of EPR parameters for MCR_{ox1}. EPR and ENDOR spectra enabled the hyperfine and nuclear quadrupole couplings of the four hydropyrrolic nitrogens to be determined. The optimized values are comparable with those given by Telser et al.[20] and show that all four nitrogens have approximately similar hyperfine couplings and thus spin densities. The hydropyrrolic nitrogen hyperfine couplings are close to those in MCR_{red1} but significantly different from those of MCR_{red2}.[49] In the latter case, one of the four hydropyrrolic hyperfine interactions is significantly smaller (A = [16, 13.5,

11.8] MHz) than the other three, indicating a large electronic or geometric distortion of F_{430} in MCR_{red2}.

Hyperfine and nuclear quadrupole interactions from the β protons (deuterons) of CoM can be used to determine key distances and angles and thus the position of CoM. Since the anisotropies of the hyperfine couplings of the protons $\beta 1$ and $\beta 2$ are significantly different, the two Ni−H distances are also different, as expected from the crystal structure of $MCR_{ox1-silent}$ (Chart 1). For a proton, the dipolar part of the hyperfine interaction can be calculated using the point−dipole model,[31]

$$\mathbf{A} = (\mathbf{g}/g_e)\sum_k \rho_k \mathbf{T}_k \tag{1a}$$

with

$$\mathbf{T}_k = (\mu_o/4\pi h)(g_e\beta_e g_n\beta_n)(3\mathbf{n}_k\mathbf{n}_k^{\dagger} - \mathbf{1})\frac{1}{r_k^3}, \tag{1b}$$

where r_k are the distances and $\mathbf{n}_k$ are the vectors between the proton ($\beta 1$ or $\beta 2$) and nuclei k (Ni, S, and N) with spin densities ρ_k. In MCR_{ox1} the distances between the unpaired electron and the $\beta 1$ and $\beta 2$ protons are relatively large (>0.25 nm), and thus the validity of the point-dipole approximation is assured. The main error is caused by the estimation of the spin density on the nickel, which was obtained by calculating the spin density on the sulfur and the four nitrogens, assuming that there are no other large couplings and that the sum adds to 100%. Thus, using $\rho(S) = 7 \pm 3\%$ (see below), $\rho(N) = 3 \pm 1\%$ (average value for each nitrogen), and $\rho(Ni) = 85 \pm 5\%$, with Ni−H distances of $r(\beta 1) \cong 0.26-0.28$ nm and $r(\beta 2) \cong 0.37-0.40$ nm, we calculated the dipole hyperfine tensors to be in the ranges $T_{calcd}(\beta 1) \cong [-(4.6-3.8), -(4.2-3.1), +(7.1-8.7)]$ MHz and $T_{calcd}(\beta 2) \cong [-(2.1-1.7), -(1.9-1.6), +(3.3-4.1)]$ MHz. The corresponding experimental values are $T(\beta 1) = [-4.6 \pm 0.4, -3.5 \pm 0.4, 8.1 \pm 0.4]$ MHz and $T(\beta 2) = [-2.0 \pm 0.4, -1.7 \pm 0.4, 3.7 \pm 0.4]$ MHz. Compared to the Ni(II) $MCR_{ox1-silent}$ crystal structure, with $r(\beta 1) = 0.30$ nm and $r(\beta 2) = 0.42$ nm, our values for MCR_{ox1} are slightly shorter. These differences are probably not significant given the error in the spin density distribution and the positioning of β protons from the crystal structure. It is however clear from our data that the angles with respect to the $\mathbf{g}_3$ axis (**z** axis) and distances between the β protons of CoM and the nickel are similar in MCR_{ox1} and $MCR_{ox1-silent}$.

The measured ^{33}S hyperfine coupling shows that the thiol sulfur of CoM is coordinated to the nickel ion of F_{430},[51] in agreement with the proposal based on cryoirradiation,[17] XAS,[18,19] and MCD[29,30] experiments. The ^{33}S hyperfine matrix is rhombic and can be split into an isotropic and two dipolar contributions

$$\mathbf{A}(^{33}S) = \begin{bmatrix} A_x \\ A_y \\ A_z \end{bmatrix} = \begin{bmatrix} 10 \\ 24 \\ 17 \end{bmatrix} = 17 + \begin{bmatrix} -0.4 \\ -0.4 \\ 0.8 \end{bmatrix}_{PD} + \begin{bmatrix} -6.6 \\ 7.4 \\ -0.8 \end{bmatrix} \text{MHz}$$

The first term is the isotropic coupling and indicates spin density in the s-orbitals. The second term is the point-dipolar contribution calculated using eq 1 and a nickel to sulfur distance of 0.24 nm determined from XAS measurements.[19] Since there is spin density on the sulfur, the point-dipole model provides only an estimate of the magnitude of this interaction. The last term is rhombic and shows that the sulfur contributes more than one p-orbital to the SOMO, since a single p-orbital contribution results in an axial interaction. The isotropic and dipolar parts of the hyperfine matrix allow the spin density ρ in the s- and p-orbitals to be estimated. Using tables in reference[52] we find ρ(s-orbital) $= 0.5 \pm 0.1\%$ and ρ(p-orbitals) $= 6 \pm 3\%$. The hyperfine interaction in MCR_{ox1} can be compared to the one of MCR_{red2}, which has the thiol(ate) sulfur of CoM coordinated to a Ni(I) ion. For MCR_{red2} we found the ^{33}S hyperfine principal values $|A(^{33}S)| = [15,15,35]$ MHz,[53] which are larger than those in MCR_{ox1}. These data suggest that the Ni−S interaction is slightly weaker in MCR_{ox1}.

The knowledge of the hyperfine couplings of the sulfur and β protons of CoM is a useful indicator of the contribution of the sulfur to the SOMO. The isotropic part of the β-proton hyperfine coupling is due to spin polarization and/or spin delocalization, is dependent upon the sulfur spin density, and in general can be positive or negative. For a spin polarization mechanism with a π and a σ contribution, the relationship between the sulfur spin density and the isotropic β-proton hyperfine coupling is given by $a_{iso}(\beta i) = [B \cos^2 \theta_i + C]\rho_s$,[54] where θ_i is the dihedral angle formed by the direction of the sulfur π-orbital axis and the C_β-$H_{\beta i}$ σ-bond axis. The coefficients $B \sim 100$ MHz and $C \sim 20$ MHz have been determined empirically. This expression is appropriate for a thiolate sulfur considered as sp^2 hybridized, with the spin polarization interaction arising largely from a single sulfur π-orbital (coefficient B) carrying most of the spin density, with a small σ contribution (coefficient C). This model is used, for example, in type I copper proteins, where the Cu(II) ion is coordinated to the thiolate sulfur of a cysteine residue, with the SOMO having a sulfur π-orbital which overlaps with the copper $d_{x^2-y^2}$ orbital. Applying this equation to MCR_{ox1}, with the dihedral angles (Ni−S−C_β−H_β) $\theta_1 = 25°$ and $\theta_2 = 140°$, and the spin density $\rho_s = 7 \pm 3\%$, yields values of $a_{iso}(\beta 1) = 5-12$ MHz and $a_{iso}(\beta 2) = 4-9$ MHz. Compared to the experimental values of $a_{iso}(\beta 1) = -2.0 \pm 0.4$ MHz and $a_{iso}(\beta 2) = -1.5 \pm 0.4$ MHz, the calculated values are significantly larger and have the opposite sign. This discrepancy points to a different mechanism than is operative in the blue copper proteins. In MCR the spin carrying sulfur orbital is not a (approximately) pure π-orbital, as is often assumed in the blue copper proteins,[55] but has contributions from an s-orbital and p-type orbitals. This picture is consistent with the sulfur hyperfine tensor with a large isotropic part and rhombic symmetry. In support of this is the approximate tetrahedral symmetry around the sulfur ($\angle$Ni−S−$C_\beta = 102.7°$) in $MCR_{ox1-silent}$. Negative a_{iso} values for the β protons can result either from spin polarization with a negative sulfur spin density or by spin delocalization from the sulfur onto the β carbon (which then has positive spin density). We expect that the large and anisotropic ^{33}S hyperfine coupling implies a positive spin

(51) Note that the anisotropic part of the ^{33}S hyperfine interaction is much larger than the through space dipole−dipole contribution and that there is a large isotropic component. These features require an overlap of S and Ni orbitals and thus a Ni−S coordination.

(52) Morton, J. R.; Preston, K. F. *J. Magn. Reson.* **1978**, *30*, 577−582.
(53) Finazzo, C.; Harmer, J.; Bauer, C.; Jaun, B.; Duin, E.; Mahlert, F.; Goenrich, M.; Thauer, R.; Van Doorslaer, S.; Schweiger, A. *J. Am. Chem. Soc.* **2003**, *125*, 4988−4989.
(54) Werst, M. M.; Davoust, C. E.; Hoffman, B. M. *J. Am. Chem. Soc.* **1991**, *113*, 1533−1538.
(55) Mouesca, J.-M.; Rius, G.; Lamotte, B. *J. Am. Chem. Soc.* **1993**, *115*, 4714−4731.

density, and we thus favor the spin delocalization mechanism. This picture is consistent with the apparent Ni(II) characteristics of MCR_{ox1} as observed in XAS, MCD, and UV−vis spectra and highlights the *noninnocent electron donating* characteristics of the sulfur ligand on the oxidation state.

It was previously shown that the EPR spectrum of MCR_{ox1} is significantly broadened by the ^{61}Ni hyperfine interaction and is thus originating from a nickel complex.[19] Based on the simulation of the ^{61}Ni CW EPR and ^{61}Ni ENDOR spectra recorded at both X- and Q-band, we were able to accurately determine this interaction (Table 1). Both the hyperfine and nuclear quadrupole interactions are axial within experimental error, with the axes of the largest principal values (A_3 and Q_3) pointing along $\mathbf{g}_3$ and thus perpendicular to F_{430}. The magnitude of the ^{61}Ni hyperfine interaction in MCR_{ox1} ($A(^{61}Ni)$ = [39, 42, 132] MHz) is significantly larger than that in MCR_{red2} ($A(^{61}Ni)$ = [39, 44, 67] MHz)[6] but is similar to that of MCR_{red1} ($A(^{61}N)$ = [52, 52, 195] MHz).[56] The large ^{61}Ni hyperfine interaction of MCR_{ox1} suggests that most of the spin density is in the Ni orbitals. Unfortunately, the Ni hyperfine interaction cannot be directly used to calculate a spin density as in the case of sulfur, since spin polarization in transition metal ions significantly influences the hyperfine couplings.[57]

The EPR data from the hydropyrrolic nitrogens and the nickel, along with the g values, indicate a SOMO with high $d_{x^2-y^2}$ character. Our ^{33}S data show that considerable spin density is transferred to the thiolate sulfur of CoM. What orbitals from Ni and S are responsible for this transfer? To discuss the possibilities it is instructive to examine the symmetry of the nickel hyperfine and nuclear quadrupole interactions, both of which are axial (symmetry ± [−1,−1,2] along the [**x**,**y**,**z**] axes). This symmetry is compatible with either a d_{z^2} orbital contribution to the SOMO, $c_1 d_{x^2-y^2} + c_2 d_{z^2}$ ($c_1 > c_2$), and/or equal contributions from both d_{xz} and d_{yz} orbitals, $c_1 d_{x^2-y^2} + c_2 d_{xz} + c_3 d_{yz}$ ($c_1 > c_2 \cong c_3$). Note that the principal values of the d-orbitals along the [**x**,**y**,**z**] axes have the following symmetries; $d_{x^2-y^2} \rightarrow$ [−1,−1,2], $d_{z^2} \rightarrow$ [1,1,−2], $d_{xz} \rightarrow$ [−1,2,−1], and $d_{yz} \rightarrow$ [2,−1,−1]; g_n is negative. The symmetry of the nickel hyperfine and nuclear quadrupole interactions rules out any significant contribution from a single d_{xz} or a single d_{yz} orbital, e.g., $c_1 d_{x^2-y^2} + c_2 d_{yz}$ ($c_1 > c_2$), as this would result in a rhombic interaction.

Mixing in of a nickel d_{z^2} orbital would result in a σ-type interaction with the sulfur s-type and/or p_z-type orbital. The contribution of a d_{z^2} orbital to the SOMO would explain the reduction in the g-value anisotropy and hyperfine anisotropy as compared to MCR_{red1} with a $d_{x^2-y^2}$ SOMO. The scheme may also provide a ligand field strong enough to result in a Ni(III) complex with the "unusal" $d_{x^2-y^2}$ SOMO. Note that the local symmetry around the Ni ion in MCR_{ox1} is strictly speaking C_1, and thus overlap between the $d_{x^2-y^2}$ and d_{z^2} orbitals is allowed. The C_1 symmetry is evident from the rhombic g-matrix and the hyperfine couplings of the four nitrogens, which are all different. In addition, π-interactions between suitable sulfur and the nickel d_{xz} and d_{yz} orbitals are also plausible. If π-interactions are significant, then approximately equal contributions from *both* d_{xz} and d_{yz} would be required to produce the experimental observed axial ^{61}Ni hyperfine and nuclear quadrupole tensors. A π-type overlap is predicted by DFT to be important for the model complex $[Ni^{III}F'_{430}SCH_3(Am)]^+$, which has a SOMO involving metal−ligand π-bonding (nickel d_{xz}, sulfur p_x, and two equatorial nitrogens with p_z orbitals) with spin densities of Ni (65%), S (14%), N (2 × 8−9%). As pointed out above, in MCR_{ox1} we would also require an approximately equal contribution from the nickel d_{yz} orbital. The rhombic sulfur hyperfine interaction, caused by an admixture of p-orbitals, suggests that there are both σ- and π-type interactions involved in the Ni−S bonding. A calculation of the electronic structure is required to discriminate between the possibilities discussed above.

One exchangeable proton, ex1, could be clearly identified, with the hyperfine parameters $a_{iso} = \pm 7.6$ MHz and $T = \mp$[2.6, −0.4, −2.3] MHz. Possible candidates for this interaction are the thiol proton of coenzyme M (CoM), the OH protons of the two tyrosine residues $Tyr^{\alpha 333}$ and $Tyr^{\beta 367}$, the lactam or C(2)-amide NH protons from F_{430}, the two protons from the axially coordinated $Gln^{\alpha' 147}$, or a proton from a water molecule close to CoM. The expected anisotropy of a thiol proton, estimated from the point-dipole model by assuming a H−S distance of 0.12 nm, is $T \cong$ [−2.3−2.3, 4.6] MHz. This interaction is significantly larger than the experimental value and thus indicates that CoM is coordinated as a thiolate, $^-$S−CoM. The lactam proton is ∼0.39 nm from the nickel, giving $T \cong$ [−1.3, −1.2, 2.5] MHz but would be expected to have a small isotropic component and thus probably contributes only to the proton "matrix" line. Protons from $Gln^{\alpha' 147}$ are ∼0.33 nm and ∼0.48 nm from the nickel, giving $T \cong$ [−2.1, −2.0, 4.1] MHz and $T \cong$ [−0.7, −0.7, 1.4] MHz, respectively. However, the assignment of ex1 to one of these $Gln^{\alpha' 147}$ protons is unlikely as we do not expect an isotropic contribution of $|a_{iso}| = 7.6$ MHz (since we would then expect to observe a corresponding $Gln^{\alpha' 147}$ nitrogen signal in our data), and second these protons are probably not accessible to D_2O since they are located deep within the protein on the distal side of F_{430}. Potentially, a water molecule near to the active site, as found in the crystal structure of $MCR_{ox1-silent}$, could be the source of the proton ex1. This would require that one of the water protons moves closer to either the sulfur or nickel to explain the hyperfine coupling. Most likely, proton ex1 is one (or both) of the tyrosine HO protons; both are quite close to the sulfur (r ∼0.23 nm) and from the point-dipole model would be expected to have $T \cong$ [−1.7, −1.3, 3.0] MHz. Since there is spin density on the thiolate sulfur, a large isotropic contribution to the proton hyperfine coupling is expected, as observed for proton ex1.

To discuss the oxidation state of MCR_{ox1} all relevant data must be considered. X-ray absorption (XA)[18,19] and UV−vis spectra[24,28] are more similar to the EPR-silent Ni(II) forms than to Ni(I) forms such as MCR_{red1}. MCD data have been interpreted in terms of a tetragonally compressed Ni(III) species or an antiferromagnetically coupled Ni(II)-thiyl radical species.[29] Craft et al.[30] interpreted their MCD spectra with time-dependent and time-independent DFT calculations and found reasonable agreement between experimental and calculated spectra with a complex that was oxidized by one electron relative to the Ni(II) ox1-silent model. Conversely, a calculation with one electron added to their ox1-silent model predicted that the additional electron is not localized on the nickel but rather on the macrocycle, a result in disagreement with both EPR and MCD

(56) Albracht, S. P. J.; Graf, E. G.; Thauer, R. K. *FEBS Lett.* **1982**, *140*, 311−313.
(57) Munzarová, M. L.; Kubáček, P.; Kaupp, M. *J. Am. Chem. Soc.* **2000**, *122*, 11900−11913.

data, providing an argument against this formulation. Moreover, in solution a one-electron reduction of the Ni(II) form yields a Ni(I) form, with an MCR_{red1}-like spectrum, and no reduction of the macrocycle occurs.[58] These considerations point toward a complex which is one electron oxidized relative to Ni(II) $MCR_{ox1-silent}$. Generation of MCR_{ox1} directly from $MCR_{ox1-silent}$ by γ-irradiation at low temperature would then require oxidation of either Ni(II) or the thiolate group, perhaps triggered by an OH radical generated from the water molecule found close to the CoM sulfur in $MCR_{ox1-silent}$. This radical would then act as an oxidizing agent.

Our EPR data provide a description of the spin density distribution and SOMO but not a direct measure of the ground-state or oxidation state; the correct MCR_{ox1} model must however have a spin density and SOMO consistent with the EPR results. The EPR data show that most of the spin density is located in the nickel $d_{x^2-y^2}$ orbital, with $7 \pm 3\%$ on the thiolate sulfur. If we accept the proposal that MCR_{ox1} is induced by oxidation, then our data favor a Ni(III) (d^7) thiolate in resonance with a thiyl radical/high-spin Ni(II) complex, $Ni^{III}-{}^{-}SR \leftrightarrow Ni^{II}-{}^{\bullet}SR$ (structure on left is dominate). The Ni(III) (d^7) thiolate formulation requires the thiolate sulfur of coenzyme M to be a strong σ-donating axial ligand that is capable of inducing a change from a SOMO with high d_{z^2} character to a SOMO with high $d_{x^2-y^2}$ character. The mechanism by which MCR_{ox1} is stabilized must come from the protein environment, since at least in solution no stable axially coordinated sulfur F_{430} model complexes could be synthesized. Important factors in the protein are the positioning of the thiolate sulfur directly above the Ni ion by the binding of the SO_3^- group of CoM to the protein, and probably also the stabilization by hydrogen bonds with $Tyr^{\alpha 333}$ and $Tyr^{\beta 367}$. Evidence for the participation of the tyrosine residues comes from the exchangeable proton(s) ex1.

(58) Piskorski, R.; Jaun, B. *J. Am.* Chem. Soc. **2003**, *125*, 13120−13125.

Conclusion

The EPR data show that MCR_{ox1} is a nickel-centered, $S = {}^1/_2$ complex, coordinated by the four hydropyrrolic nitrogens, the sulfur of ^-S-CoM, and presumably the oxygen from the $Gln^{\alpha' 147}$. The SOMO is essentially a nickel $d_{x^2-y^2}$ orbital with contributions from the four hydropyrrolic nitrogens and the thiolate sulfur of CoM. The thiolate sulfur has $7 \pm 3\%$ of the spin density. The Ni−S coordination potentially involves a two-center two-electron σ-bond, with the sulfur acting as an electron donor. This spin density distribution and bonding highlight the noninnocent electron donating characteristics of the sulfur ligand on the oxidation state, providing a rationale for the apparent Ni(II) like spectra observed with UV−vis, MCD, and XA spectroscopy. The hyperfine and nuclear quadrupole parameters listed in Table 1 provide data that can be used to judge the accuracy of a calculation of the electronic and geometric structure, for example, from DFT. The distance to the β protons (or the dipolar part of the hyperfine interaction itself) can be a useful constraint in any geometry optimization of a proposed structure. This constraint helps to describe the influence of the surrounding protein on the coordination, since it forces CoM to be orientated in a predefined way (Chart 1). Assuming that MCR_{ox1} is one electron oxidized relative to the Ni(II) form, our data favor a description in terms of a Ni(III) (d^7) thiolate complex in resonance with a thiyl radical/high-spin Ni(II) complex, $Ni^{III}-{}^{-}SR \leftrightarrow Ni^{II}-{}^{\bullet}SR$.

Acknowledgment. This work was supported by the Swiss National Science Foundation, by the Max Planck Society, and by the Fonds der Chemischen Industrie.

Supporting Information Available: Figures S1 to S6. This material is available free of charge via the Internet at http://pubs.acs.org.

JA053794W